NANO LETTERS

pubs.acs.org/NanoLett Letter

Engineering Artificial Protrusions of Zn Anodes for Aqueous Zinc Batteries

Jifei Sun,[†] Xinhua Zheng,[†] Zhengxin Zhu, Mingming Wang, Yan Xu, Ke Li, Yuan Yuan, Mingyan Chuai, Zaichun Liu, Taoli Jiang, Hanlin Hu,* and Wei Chen*

Cite This: https://doi.org/10.1021/acs.nanolett.4c06347 Read Online

ACCESS | Metrics & More | Article Recommendations | Supporting Information

ABSTRACT: Uncontrollable dendrite growth can jeopardize the cycle life of aqueous Zn batteries. Here, we propose a general strategy of engineering artificial protrusions (APs) on the electrode surface to regulate the distribution of the electrode interface electric field and induce stable Zn plating/stripping for Zn batteries. The junction-free AP-Cu network is constructed on Cu foil by an ultrafast Joule-heating-welding method. COMSOL simulation reveals that a stronger microelectric field is formed around the individual AP, which can effectively regulate a uniform nucleation of Zn on the AP-Cu network. Guided by the structural advantages of the AP design, the AP-Cu||Zn cell delivers an average Coulombic efficiency (CE) of 99.85% at 2 C with an areal capacity of 1.77 mAh cm^{-2} for over 3000 cycles. Moreover, the AP design enables stable cycling of both Zn|AP-Cu||V_2O_5 and anode-free AP-Cu||Br_2 full cells, providing a promising strategy for the development of high-performance energy storage devices.

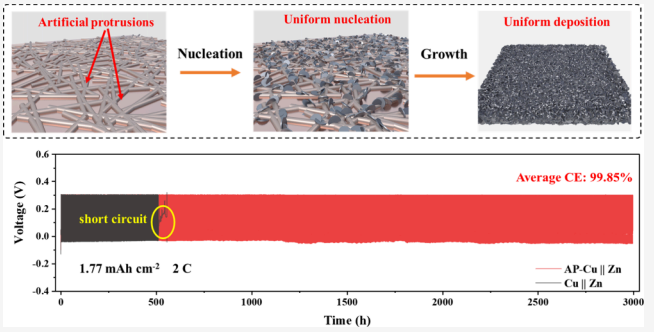

KEYWORDS: *Zn anode, dendrite-free, artificial protrusion, Joule-heating, Cu nanowires, large-scale energy storage*

Downloaded via SHANXI UNIV on April 24, 2025 at 07:43:19 (UTC).
See https://pubs.acs.org/sharingguidelines for options on how to legitimately share published articles.

With the fast development of sustainable yet intermittent wind and solar energies, electrochemical energy storage technologies have attracted much attention to integrating those renewable energies into electric grids.[1−3] Aqueous Zn-ion batteries (AZIBs) are emerging as one of the most promising candidates for grid-scale applications due to their merits of high theoretical capacity (820 mAh g^{-1}), low cost, and intrinsic high safety.[4−14] However, AZIBs still face the inherent issue of dendrite growth from the Zn anodes, which leads to low Coulombic efficiency (CE) and even short-circuiting of the battery in prolonged cycle.[15,16] Numerous research studies have demonstrated that the dendrite growth is driven by "tip effect".[17,18] During the Zn plating process, uneven Zn deposition causes the formation of surface protrusions. These unevenly distributed surface protrusions create a higher electric field around them, resulting in the preferential accumulation and deposition of Zn on those protrusions, ultimately leading to the formation of Zn dendrites. Therefore, numerous endeavors have been exerted to inhibit the formation of surface protrusion or reduce the effect of surface protrusion in different ways, including electrolyte modification,[19−24] artificial SEI construction,[25−29] and electrode design.[30−32]

Among those strategies, the texture design of electrode surface is one of key research directions, which can regulate the distribution and crystal orientation of Zn plating, thus alleviating the detrimental effects of "tip effect".[33] For instance, a zincophilic interfacial layer was constructed on the electrode surface to reduce the nucleation barrier, thus reducing the uncontrollable protrusion formation.[34−37] The pretreatment of Zn electrode with more exposure of the (002) surface or the materials with low (002) crystal lattice distortion index was used to induce Zn plating along (002) crystal facet by the epitaxial growing technology, thereby decreasing the formation of surface Zn protrusions.[38−41] Besides, researchers designed a ridge-like surface texture on the electrode and induced Zn plating at the concavity areas. The concave voids not only provide sufficient growing space but also can alleviate the dendrites growing directly toward the cathode, thus reducing the effect of surface protrusion.[42−44] Although these texture design strategies are effective in alleviating the dendrite growth of Zn anodes, it is still necessary to study the Zn plating process and develop new methods to suppress dendrite growth, which can provide more options for the commercialization of Zn batteries.

The typical process of Zn plating can be roughly divided into three consecutive stages, i.e., Zn nucleation, nucleus growth, and further Zn growth. Several studies have shown that the uniform nucleation of Zn at the initial plating stage is beneficial to guide

Received: December 13, 2024
Revised: April 14, 2025
Accepted: April 17, 2025

ACS Publications © XXXX American Chemical Society

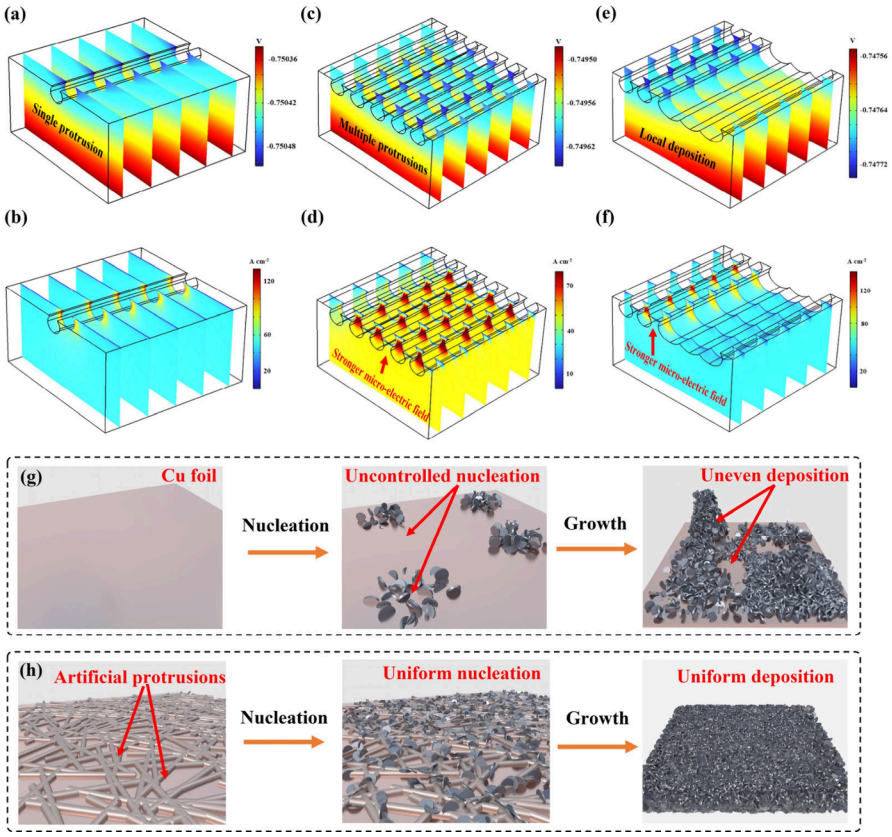

Figure 1. Simulation and working mechanism of the AP design. COMSOL simulation of the electric field distribution at the electrode/electrolyte interface with (a) one artificial protrusion, (c) multiple artificial protrusions, and (e) the localized Zn deposition. COMSOL simulation of the plating current intensity distribution at the electrode/electrolyte interface with (b) one artificial protrusion, (d) multiple artificial protrusions, and (f) the localized Zn deposition. Schematic illustrations of Zn deposition on the electrode surface (g) without and (h) with artificial protrusions.

the nucleus growth to maintain its uniformity and ultimately form a uniform plating layer.[34,45,46] To obtain evenly distributed Zn embryos during the nucleation stage, a new design idea for electrode surface texture by rationally utilizing the "tip effect" is proposed in this work. Different from the above strategies to reduce surface protrusions or construct a uniform electric field distribution by using a 3D electrode, we propose a general strategy of engineering an artificial protrusions (AP) network on the electrode surface to induce the homogeneous Zn nucleation and growth. We take advantage of the high curvature surface of these APs, which can construct a stronger microelectric field around them, thereby inducing Zn nucleation on these APs and avoiding uncontrollable Zn nucleation and growth on the electrode surface. To prove the advantages of our strategy, a Cu foil electrode with the AP design (AP-Cu), generated by a facile Joule-heating welding process, is used as a model. Benefiting from the robust AP structure design, the Zn plating layer on the AP-Cu electrode is more uniform than that on the pristine Cu foil electrode. The asymmetric AP-Cu||Zn cell shows an average Coulombic efficiency (CE) of 99.85% at 2 C with an areal capacity of 1.77 mAh cm^{-2} for over 3000 cycles. Further, the fabricated anode-free Zn||Br_2 battery using the AP-Cu anode shows much-improved cycle stability, which delivers a high discharge voltage of ~1.6 V and a 97% energy retention after 900 cycles with an areal capacity of 2 mAh cm^{-2} at 5 C.

SIMULATION AND DESIGN PRINCIPLE OF AP DESIGN

Before the experimental verification of the AP design, COMSOL simulations of the distributions of the surface electric field and the electric current density were implemented to explore the working mechanism of the AP design and guide the construction of the AP-Cu electrode. As shown in Figure S1a and Figure 1a,b, the electric field strength and the plating current intensity around the AP (i.e., high curvature surface) are obviously stronger than the flat area. The simulated results suggest that a stronger microelectric field is constructed around the AP, where the deposition of Zn is prone to occur. The simulation results are also consistent with the previously reported literature.[47] According to the simulation results of electrode with one AP, if numerous APs are evenly constructed on the electrode surface, the nucleation behavior of Zn should be effectively regulated to plate on those APs under the effect of stronger microelectric field around those APs, which can avoid the uncontrollable nucleation and dendrite growth. To prove this hypothesis, multiple artificial protrusions were evenly constructed on the electrode surface (Figure S1b). The simulated distributions of surface electric field (Figure 1c) and plating current intensity (Figure 1d) show that the stronger microelectric field is formed around individual AP, suggesting that Zn can be effectively regulated to nucleate on those artificial protrusions. Besides, the surface electric field distribution of electrode with multiple APs is also more uniform than that of electrode with one AP as shown in Figure S3. Based on the above results, it can be inferred that the uniform and dense single layer AP network constructed on

https://doi.org/10.1021/acs.nanolett.4c06347
Nano Lett. XXXX, XXX, XXX−XXX

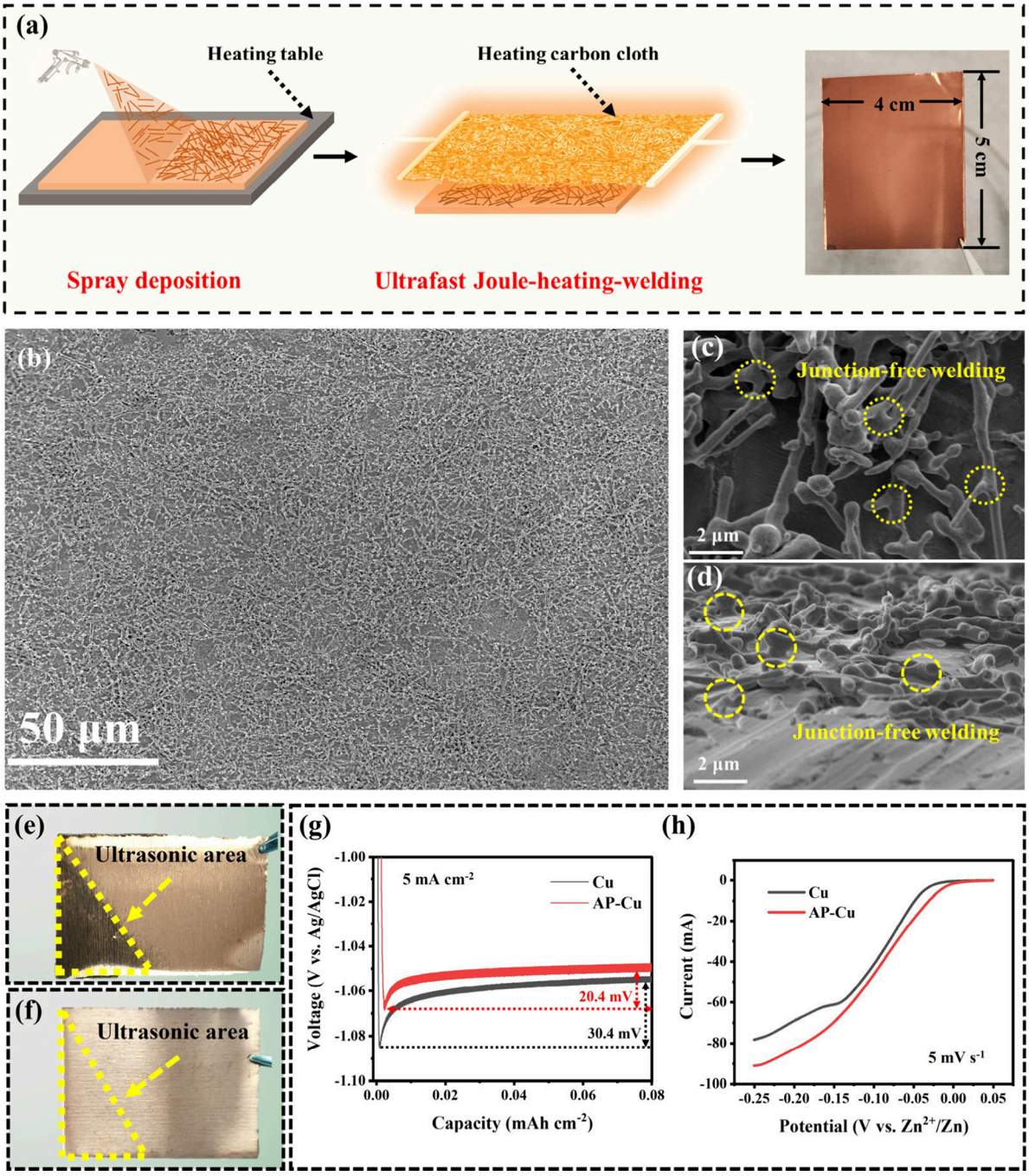

Figure 2. Preparation and characterization of AP-Cu. (a) Schematic of the preparation process of AP-Cu. (b) SEM image of synthesized AP-Cu. Magnified images of the junction-free welding (c) between Cu nanowires and Cu nanowires, and (d) Cu nanowires and Cu foil. The structure stability test of AP electrode (e) before and (f) after ultrafast Joule-heating-welding treatment. (g) Voltage profiles of galvanostatic Zn plating on the pristine Cu and AP-Cu electrodes. (h) Linear polarization curves of the pristine Cu and AP-Cu electrodes.

the electrode surface can introduce uniform Zn nucleation, resulting in uniform Zn plating, as illustrated in Figure 1g,h.

Apart from the ability of AP network to induce uniform nucleation and growth of Zn, the situation in which localized Zn deposition occurs on the electrode surface with AP design is also considered and simulated by COMSOL. One of the reasons for this situation is insufficient external energy (low plating current density) providing for Zn plating, which can cause a reduction in the number of nucleus and poor nucleation uniformity, resulting in the localized Zn deposition and growth of dendrite.[37] As displayed in Figure S2 and Figure 1e,f, the microelectric field strength and the plating current intensity around the AP without Zn deposition are obviously stronger than that of the AP with Zn deposition. It suggests that the external energy for Zn deposition will be more distributed on the AP without Zn deposition, which can activate extra nucleation sites to induce preferential deposition of Zn on these APs. Hence, this "self-activation" process may regulate the Zn deposition behavior and promote the uniformity of Zn deposition on the AP electrode design, even if uneven local zinc deposition occurs.

https://doi.org/10.1021/acs.nanolett.4c06347
Nano Lett. XXXX, XXX, XXX−XXX

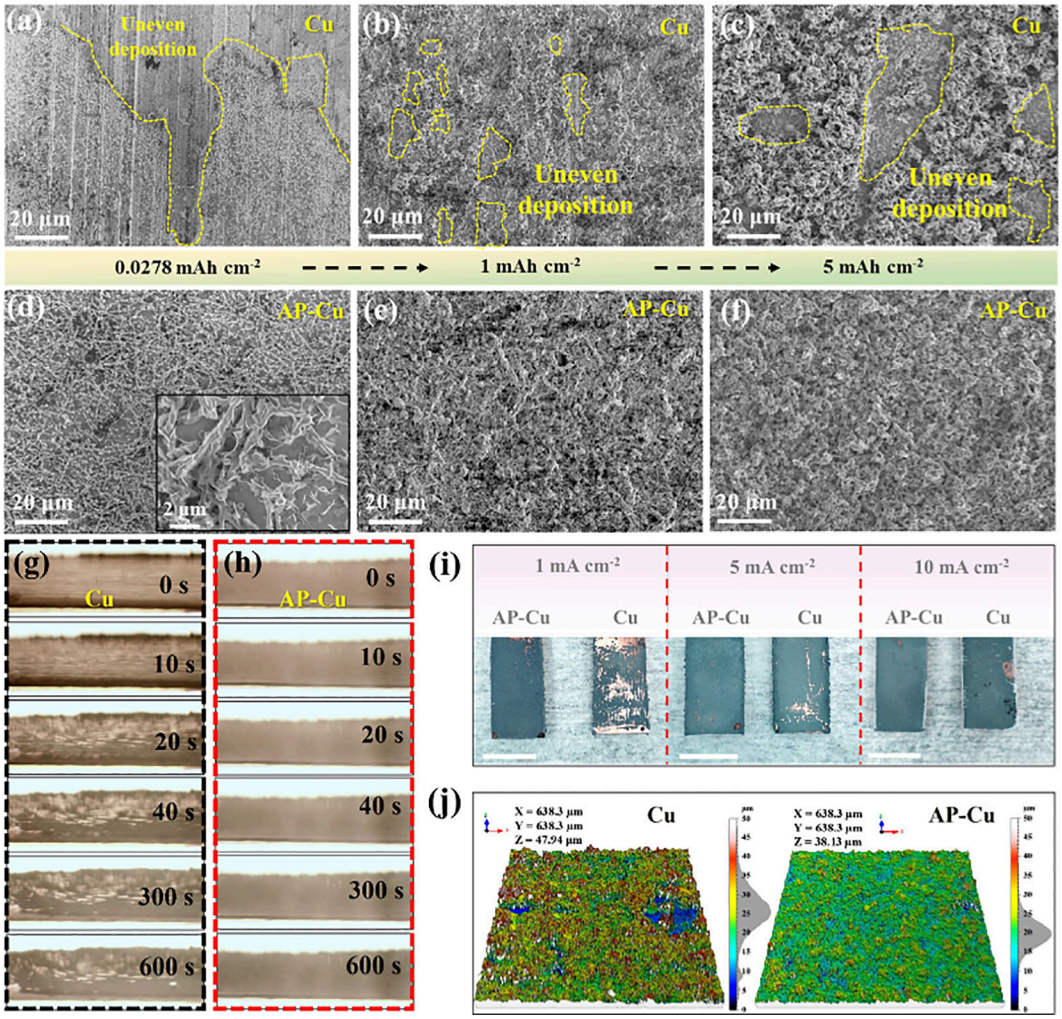

Figure 3. Morphology of Zn plating on pristine Cu and AP-Cu substrates. SEM images of Zn plated on (a–c) Cu and (d–f) AP-Cu with different areal capacities at 10 mA cm^{-2}. In situ optical microscope visualization of Zn plated on (g) Cu and (h) AP-Cu at 10 mA cm^{-2}. (i) The morphology of 10 mAh cm^{-2} of Zn plated on Cu and AP-Cu electrodes at different plating current densities. Scale bars: 5 mm. (j) Confocal laser scanning microscope images of Zn plated on Cu and AP-Cu at 10 mA cm^{-2} with a high areal capacity of 10 mAh cm^{-2}.

PREPARATION AND CHARACTERIZATION OF AP-CU

To experimentally prove this concept, the synthesized Cu nanowires[48,49] were chosen as artificial protrusions (Figure S4). The AP-Cu electrode was facilely prepared by two steps of spray deposition and a well-established Joule-heating welding,[50,51] as illustrated in Figure 2a and Figure S5. Before Joule heating-welding, the Cu nanowires are in a stacked state on the Cu surface without robust connection (Figure S6), which can be easily removed from Cu foil by the ultrasonic washing (Figure 2e). After 4 s of ultrafast Joule-heating-welding treatment, the synthesized AP-Cu exhibits a morphology of uniform distribution of the junction-free AP network (Figure 2b). The magnified SEM image of AP-Cu shows that Cu nanowires are welded together with each other and with the Cu substrate (Figure 2c,d), which helps to reduce the contact resistance of electrode.[52] Meanwhile, the APs remain on the Cu foil after ultrasonic washing (Figure 2f), demonstrating robust structure stability. The XRD pattern of the AP-Cu shows the same crystal plane orientation as the pristine Cu (Figure S7). Furthermore, the nucleation overpotential and deposition kinetics of Zn on the AP-Cu electrode were characterized. Benefiting from the AP design, Zn deposited on AP-Cu electrode has a lower nucleation overpotential and better deposition kinetics than these of Zn deposited on pristine Cu electrode (Figure 2g,h), suggesting that a uniform Zn plating layer on the AP-Cu can be expected.

MORPHOLOGY OF ZN ELECTRODEPOSITION ON PRISTINE CU AND AP-CU

To reveal the nucleation and growth process of Zn on pristine Cu and AP-Cu, the surface morphology of pristine Cu and AP-Cu with different areal capacities of Zn plating was observed by SEM. On the pristine Cu surface, Zn is unevenly deposited at the initial nucleation stage (Figure 3a). With the increase of deposited areal capacity, those unevenly distributed nuclei of Zn will continue to grow, leading to the deteriorated uniformity of Zn plating (Figure 3b and Figure 3c). In comparison, the AP-Cu shows uniform nucleation at the initial stage. Moreover, it is further revealed that Zn was evenly deposited on the surface of artificial protrusions (Figure 3d), which is consistent with the simulated results of COMSOL. Guided by homogeneous nucleation, the morphology of Zn deposited on the AP-Cu is uniform even at a higher deposition areal capacity (Figure 3e,f). Furthermore, the in situ observation was also employed to

https://doi.org/10.1021/acs.nanolett.4c06347
Nano Lett. XXXX, XXX, XXX−XXX

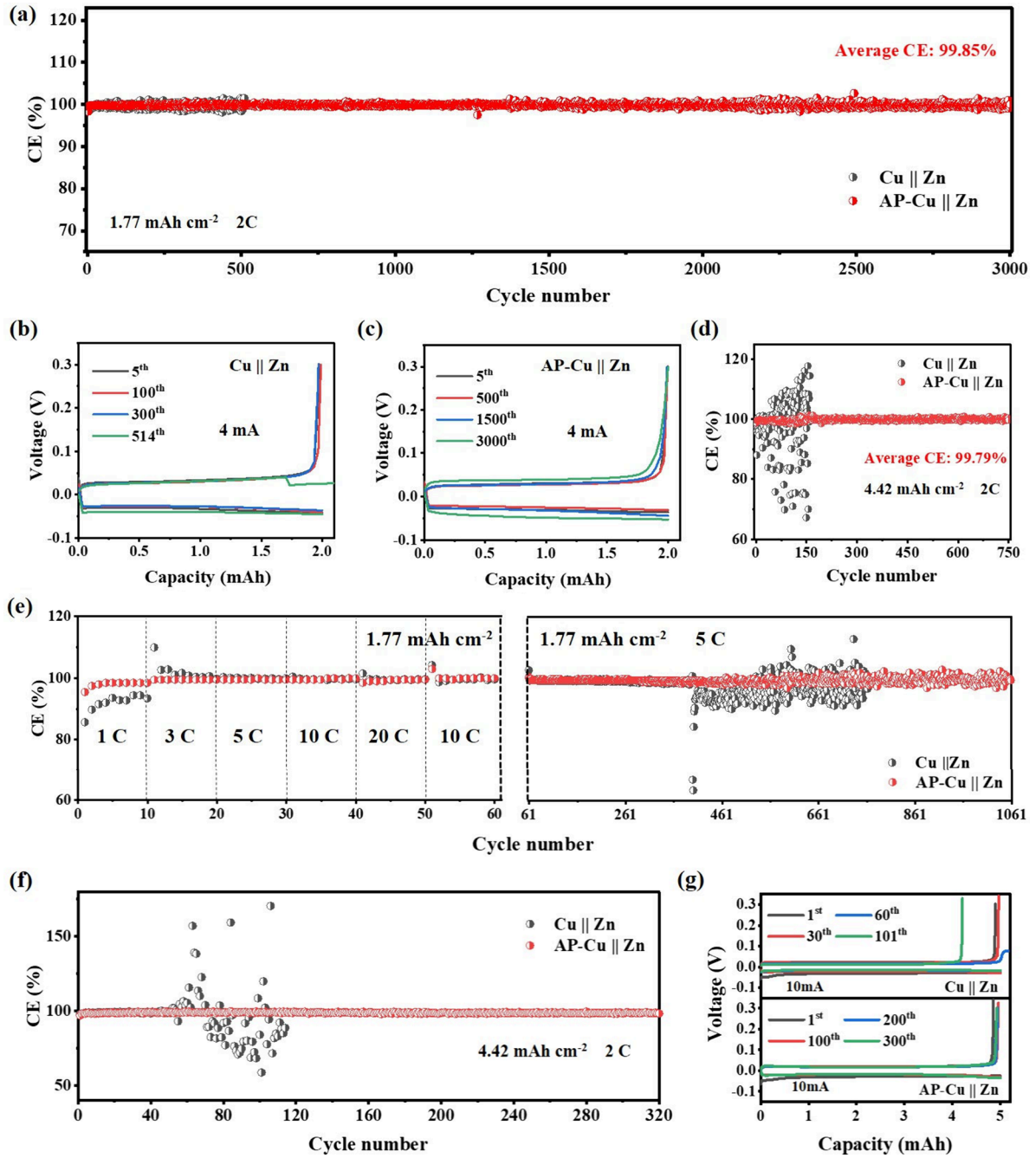

Figure 4. Electrochemical performance of the asymmetric AP-Cu||Zn cell. (a) Coulombic efficiency of Cu||Zn and AP-Cu||Zn cells. Voltage profiles of (b) Cu||Zn and (c) AP-Cu||Zn cells. (d) Coulombic efficiency of Cu||Zn and AP-Cu||Zn cells with a high areal capacity. (e) Coulombic efficiency of Cu||Zn and AP-Cu||Zn cells at different rates. (f) Coulombic efficiency and (g) the corresponding voltage profiles of Cu||Zn and AP-Cu||Zn cells in 2 M $ZnBr_2$ electrolyte.

monitor the Zn plating process in a homemade transparent reactor (Figure S8). As shown in Figure 3g, the inhomogeneous nucleation of Zn was observed on the pristine Cu substrate at the initial deposition stage. With the increase of deposition time, Zn^{2+} ions are attracted and deposited on the initial nucleation sites, leading to uneven Zn plating (Figure S9a and Supporting Information Video 1). In sharp contrast, uniform Zn deposition was observed on the substrate of AP-Cu throughout the deposition process (Figure 3h and Supporting Information Video 2). The flat and dense Zn deposition on AP-Cu (Figure S9b) demonstrates the excellent capability in the regulation of homogeneous nucleation and growth.

Furthermore, the effect of external energy intensity (i.e., plating current density) providing for Zn nucleation and growth on the morphology of Zn plating on pristine Cu and AP-Cu was also investigated. Compared to uniform deposition of Zn on AP-Cu, the uniformity of Zn deposited on pristine Cu deteriorates with a decrease in plating current density (Figure 3i). It is attributed to the decrease of nuclei number with the decrease of plating current density.[46,53] However, the uniform Zn deposition on AP-Cu at low plating current densities can be ascribed to the "self-activation" phenomenon of the AP structure, as illustrated in Figure 1e,f. In addition, although the uniformity of Zn deposition on the pristine Cu has been greatly

https://doi.org/10.1021/acs.nanolett.4c06347
Nano Lett. XXXX, XXX, XXX−XXX

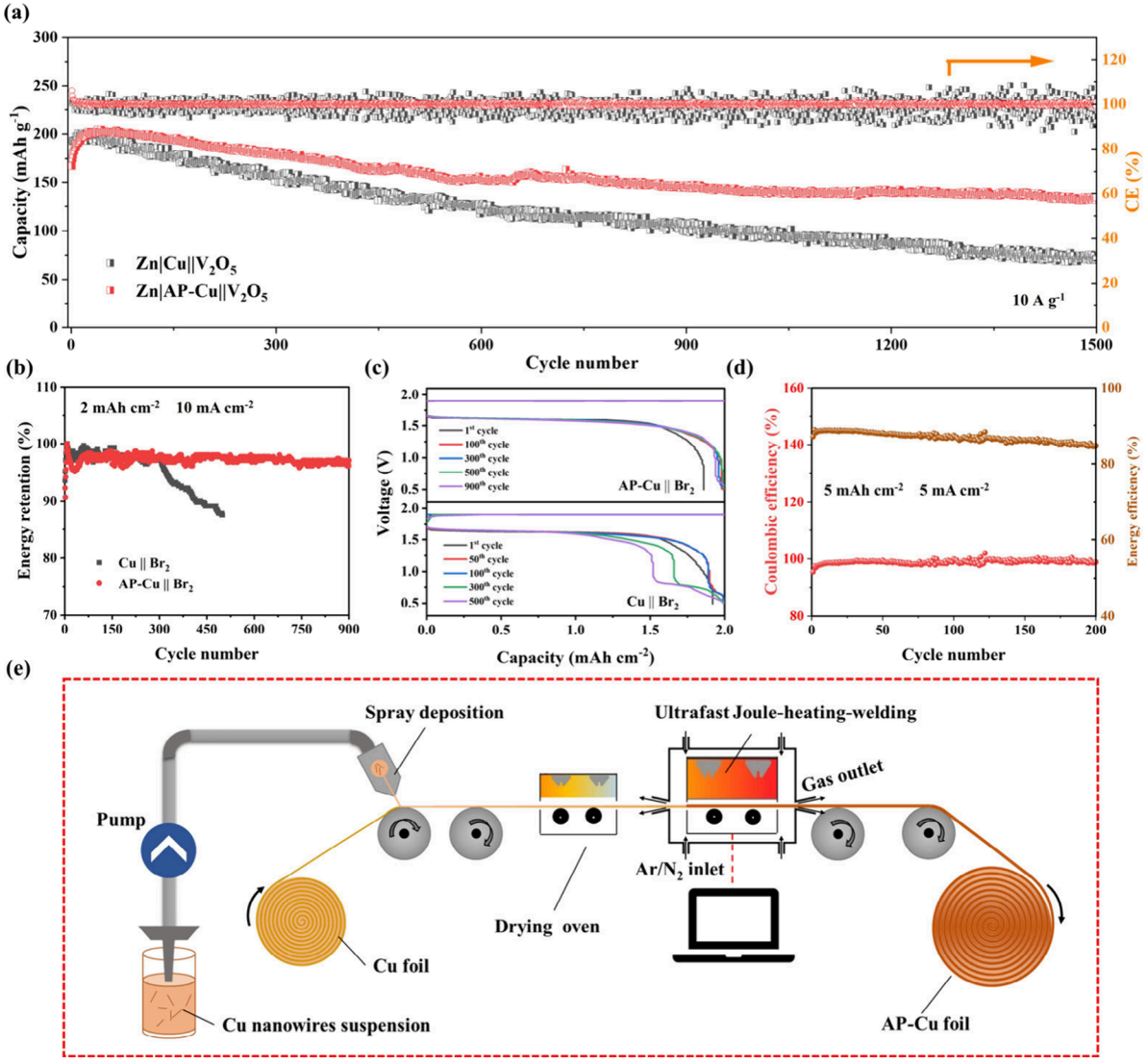

Figure 5. Electrochemical performance of AP-Cu based Zn full cells. (a) Long-term cycle performance of the Zn|Cu||V_2O_5 and Zn|AP-Cu||V_2O_5 batteries. (b) Long-term cycle performance and (c) corresponding voltage profiles of the anode-free Zn||Br_2 batteries. (d) Long-term cycle performance of the AP-Cu||Br_2 battery with an areal capacity of 5 mAh cm^{-2} at 1 C. (e) Schematic of scalable production of AP-Cu by a roll-to-roll process.

improved at the high plating current of 10 mA cm^{-2}, the 3D morphology of Zn deposited on the pristine Cu and AP-Cu characterized by a confocal laser scanning microscope shows a stark contrast, as shown in Figure 3j. The 3D morphology of Zn plated on pristine Cu exhibits an uneven Zn deposition, and the height distribution curve shows a wide height distribution from 5 to over 40 μm. In contrast, the 3D morphology of Zn plated on AP-Cu shows a relatively flat surface, and the height distribution is concentrated within a smaller range from 15 to over 25 μm compared with that of Zn plated on pristine Cu. Based on those results, improved electrochemical performance with the AP-Cu electrode can be expected.

ELECTROCHEMICAL PERFORMANCE OF AP-CU ELECTRODE

To evaluate the effect of the AP on the reversibility of Zn plating/stripping, CE measurements of Cu||Zn and AP-Cu||Zn cells were carried out. As shown in Figure 4a,b, the Cu||Zn cell only exhibits a cycle life of around 500 h. In contrast, the AP-Cu||Zn cell shows an eye-catching cycle life of more than 3000 cycles (~3000 h) with an average CE of 99.85% (Figure 4a). The voltage profile of the AP-Cu||Zn cell shows a stable charge−discharge process (Figure 4c and Figure S10). Moreover, the Cu||Zn cell exhibits an unstable cycle performance with a high areal capacity of 4.42 mAh cm^{-2}, while the AP-Cu||Zn cell shows an excellent reversibility over 750 cycles with an average CE of 99.79% (Figure 4d and Figure S12). The improved electrochemical performances of the AP-Cu||Zn cell also exhibit advantages over those of previously reported studies (Table S1), which demonstrates the application potential of the AP design.

The AP-Cu||Zn cell was further tested at different rates. As shown in Figure 4e and Figure S12a, the Cu||Zn cell shows a lower CE at 1 C, which should be attributed to the few numbers of nuclei at low plating current densities, leading to the deterioration of the uniformity of Zn plating and causing incomplete stripping or forming "dead" Zn. Benefiting from the regulation of AP, the AP-Cu||Zn cell delivers a higher CE at a low plating current density than that of the Cu||Zn cell. Meanwhile, the AP-Cu||Zn cell shows a lower overpotential than the Cu||Zn cell at high rates (Figure S12b). After the rate tests,

https://doi.org/10.1021/acs.nanolett.4c06347
Nano Lett. XXXX, XXX, XXX−XXX

the asymmetric cells continued to cycle for long cycle tests. As displayed in Figure 4e and Figure S12c, the CE of Cu||Zn cell has large fluctuations after 300 cycles, and the short-circuit signal was observed after 700 cycles. The fluctuation of the CE should be attributed to the polarization of the battery caused by uneven Zn plating on the surface of the Cu electrode. Because of the uneven Zn plating on the surface of the Cu electrode, the polarization of the Cu||Zn cell is relatively large and damages the discharge efficiency. Due to the relatively low discharge efficiency, the residual Zn will accumulate on the anode, which may improve the uniformity of the plated Zn on the electrode surface to a certain extent, leading to the polarization decrease and discharge efficiency increase, thus causing the fluctuation. In contrast, the AP-Cu||Zn cell displays a stable cycle performance over 1000 cycles and delivers an average CE of 99.48% (Figure S12d). To verify the universality of the AP design, the AP-Cu||Zn cell was also tested in a $ZnBr_2$ electrolyte, which also shows an enhanced plating/stripping reversibility, as shown in Figure 4f,g.

ELECTROCHEMICAL PERFORMANCE OF AP-CU BASED ZN FULL CELLS

Two different full cells of Zn|AP-Cu||V_2O_5 cell and anode-free Zn||Br_2 cell were assembled to test their electrochemical performance. Benefiting from the uniformity of the Zn|AP-Cu electrode (Figure S13c), the Zn|AP-Cu||V_2O_5 cell has a lower charge transfer resistance (4.89 Ω) than that of the Zn|Cu||V_2O_5 cell (7.72 Ω) (Figure S13d,e). Meanwhile, the Zn|AP-Cu||V_2O_5 cell also has a higher discharge voltage platform and capacity (Figure S13f) than the Zn|Cu||V_2O_5 cell. Besides, the Zn|AP-Cu||V_2O_5 cell also exhibits a 60% capacity retention when the discharge current increases from the 0.5 to 10 A g^{-1} (Figure S14), significantly better than that of the Zn|Cu||V_2O_5 cell (48%). In the case of the long-term cycling performance (Figure 5a), the Zn|AP-Cu||V_2O_5 cell shows a capacity of 135 mAh g^{-1} after 1500 cycles, while the capacity of the Zn|Cu||V_2O_5 cell drops quickly to 71 mAh g^{-1}, demonstrating the greatly improved electrochemical performance with the assistance of the AP design.

Further, an anode-free Zn||Br_2 full cell was also assembled to verify the advantages of AP design (AP-Cu||Br_2 or Cu||Br_2) (Figures S15 and S16). With the assistance of the APs, the AP-Cu||Br_2 battery delivers 97% energy retention after 900 cycles (Figure 5b). The voltage profiles of AP-Cu||Br_2 battery also exhibits a stable charge−discharge process with a high average discharge voltage of ∼1.6 V (Figure 5c). In contrast, the energy retention of the Cu||Br_2 battery decreases quickly after ∼300 cycles. The voltage profiles of the Cu||Br_2 battery show that a platform located on ∼0.7 V appears after 300 cycles, which is attributed to the Cu stripping during the discharge process. Because the "dead Zn" is formed on the pristine Cu electrode due to the uneven deposition, the residual $TPABr_3$ accumulated in the previous cycle will react with Cu and exhibit an ∼0.7 V discharge platform. To explore the practicability of the AP-Cu||Br_2 battery for energy storage applications, long-term cycling tests under high areal capacities were carried out. As shown in Figure 5d, the AP-Cu||Br_2 battery with an areal capacity of 5 mAh cm^{-2} shows a stable cycle over 200 cycles, which delivers an average Coulombic efficiency of 98.99% and an average energy efficiency of 86.92%. The voltage profiles also show a high average discharge voltage of ∼1.63 V (Figure S17). The above full cell tests indicate that the electrode design of APs in this work provides a promising strategy toward practical high-performance aqueous Zn batteries. Based on the convenient preparation process, robust structural stability, and enhanced electrochemical performance of AP design, we also put forward the concept of large-scale production of AP-Cu through a "roll-to-roll" process, as illustrated in Figure 5e, exhibiting great practical application potential.

In summary, we have rationally designed Zn anodes with artificial protrusions to achieve reversible and stable Zn plating and stripping for Zn batteries. The COMSOL simulation revealed that a stronger microelectric field was constructed around the AP, which can effectively induce uniform nucleation and growth of Zn. Benefiting from the advantages of AP design, the AP-Cu||Zn cell delivered a stable cycling life for over 3000 cycles with an average Coulombic efficiency of 99.85% at 1.77 mAh cm^{-2}. Further, the assembled Zn|AP-Cu||V_2O_5 and anode-free AP-Cu||Br_2 full cells showed an enhanced electrochemical performance. Moreover, the scalable production of AP-Cu can also be achieved by a roll-to-roll process, which shows great promise in the development of rechargeable aqueous Zn batteries for large-scale energy storage applications.

ASSOCIATED CONTENT

Supporting Information

The Supporting Information is available free of charge at https://pubs.acs.org/doi/10.1021/acs.nanolett.4c06347.

Experimental details, characterizations, COMSOL simulation, and supplementary figures (PDF)

Video 1 showing Zn plating on Cu electrode, in which two-electrode (Zn foil and Cu foil) configuration was applied for the in situ optical microscopy test and in which galvanostatic deposition was performed by an electrochemical workstation (CHI660E) under a current density of 10 mA cm^{-2} (MP4)

Video 2 showing Zn plating on AP-Cu electrode, in which two-electrode (Zn foil and AP-Cu foil) configuration was applied for the in situ optical microscopy test and in which galvanostatic deposition was performed by an electrochemical workstation (CHI660E) under a current density of 10 mA cm^{-2} (MP4)

AUTHOR INFORMATION

Corresponding Authors

Hanlin Hu − *Hoffmann Institute of Advanced Materials, Shenzhen Polytechnic University, Shenzhen, Guangdong 518000, China;* orcid.org/0000-0001-5617-0998; Email: hanlinhu@szpt.edu.cn

Wei Chen − *Department of Applied Chemistry, School of Chemistry and Materials Science, Hefei National Research Center for Physical Sciences at the Microscale, University of Science and Technology of China, Hefei, Anhui 230026, China;* orcid.org/0000-0002-8018-4529; Email: weichen1@ustc.edu.cn

Authors

Jifei Sun − *Hoffmann Institute of Advanced Materials, Shenzhen Polytechnic University, Shenzhen, Guangdong 518000, China; Department of Applied Chemistry, School of Chemistry and Materials Science, Hefei National Research Center for Physical Sciences at the Microscale, University of Science and Technology of China, Hefei, Anhui 230026, China;* orcid.org/0000-0002-0877-900X

https://doi.org/10.1021/acs.nanolett.4c06347
Nano Lett. XXXX, XXX, XXX−XXX

Xinhua Zheng − *Department of Applied Chemistry, School of Chemistry and Materials Science, Hefei National Research Center for Physical Sciences at the Microscale, University of Science and Technology of China, Hefei, Anhui 230026, China*
Zhengxin Zhu − *Department of Applied Chemistry, School of Chemistry and Materials Science, Hefei National Research Center for Physical Sciences at the Microscale, University of Science and Technology of China, Hefei, Anhui 230026, China*
Mingming Wang − *Department of Applied Chemistry, School of Chemistry and Materials Science, Hefei National Research Center for Physical Sciences at the Microscale, University of Science and Technology of China, Hefei, Anhui 230026, China*
Yan Xu − *Hoffmann Institute of Advanced Materials, Shenzhen Polytechnic University, Shenzhen, Guangdong 518000, China; Department of Applied Chemistry, School of Chemistry and Materials Science, Hefei National Research Center for Physical Sciences at the Microscale, University of Science and Technology of China, Hefei, Anhui 230026, China*
Ke Li − *Department of Applied Chemistry, School of Chemistry and Materials Science, Hefei National Research Center for Physical Sciences at the Microscale, University of Science and Technology of China, Hefei, Anhui 230026, China*
Yuan Yuan − *Department of Applied Chemistry, School of Chemistry and Materials Science, Hefei National Research Center for Physical Sciences at the Microscale, University of Science and Technology of China, Hefei, Anhui 230026, China*
Mingyan Chuai − *Department of Applied Chemistry, School of Chemistry and Materials Science, Hefei National Research Center for Physical Sciences at the Microscale, University of Science and Technology of China, Hefei, Anhui 230026, China*
Zaichun Liu − *Department of Applied Chemistry, School of Chemistry and Materials Science, Hefei National Research Center for Physical Sciences at the Microscale, University of Science and Technology of China, Hefei, Anhui 230026, China*
Taoli Jiang − *Department of Applied Chemistry, School of Chemistry and Materials Science, Hefei National Research Center for Physical Sciences at the Microscale, University of Science and Technology of China, Hefei, Anhui 230026, China*

Complete contact information is available at:
https://pubs.acs.org/10.1021/acs.nanolett.4c06347

Author Contributions

[†]Jifei Sun and Xinhua Zheng contributed equally to this paper.

Notes

The authors declare no competing financial interest.

■ ACKNOWLEDGMENTS

This work was financially supported by the National Natural Science Foundation of China (Grants 52471242 and 92372122), the Fundamental Research Funds for the Central Universities (Grants KY2060000150, WK2060000040, and GG2060127001), and the Scientific Research Startup Fund for Shenzhen High-Caliber Personnel of Shenzhen Polytechnic (Grants 6022310038k and 6022310049k). The authors are thankful for the support from USTC Center for Micro and Nanoscale Research and Fabrication. This work was partially carried out at the Instruments Center for Physical Science, University of Science and Technology of China.

■ REFERENCES

(1) Gür, T. M. Review of electrical energy storage technologies, materials and systems: challenges and prospects for large-scale grid storage. *Energy Environ. Sci.* **2018**, *11*, 2696−2767.
(2) Castillo, A.; Gayme, D. F. Grid-scale energy storage applications in renewable energy integration: A survey. *Energy Convers. Manage.* **2014**, *87*, 885−894.
(3) Yang, Z.; Zhang, J.; Kintner-Meyer, M. C. W.; Lu, X.; Choi, D.; Lemmon, J. P.; Liu, J. Electrochemical Energy Storage for Green Grid. *Chem. Rev.* **2011**, *111*, 3577−3613.
(4) Wang, M.; Meng, Y.; Sajid, M.; Xie, Z.; Tong, P.; Ma, Z.; Zhang, K.; Shen, D.; Luo, R.; Song, L.; Wu, L.; Zheng, X.; Li, X.; Chen, W. Bidentate Coordination Structure Facilitates High-Voltage and High-Utilization Aqueous Zn-I_2 Batteries. *Angew. Chem., Int. Ed.* **2024**, *63*, No. e202404784.
(5) Lv, W.; Shen, Z.; Liu, J.; Li, X.; Ding, F.; Zhang, D.; Miao, L.; Lyu, X.; Li, R.; Wang, M.; Li, Y.; Meng, J.; Xu, C. In situ synthetic C encapsulated δ-MnO2 with O vacancies: a versatile programming in bio-engineering. *Sci. Bull.* **2025**, *70* (2), 203−211.
(6) Wei, T.; Mo, L.; Ren, Y.; Zhang, H.; Wang, M.; He, Y.; Tan, P.; Li, Z.; Chen, W.; Hu, L. Non-sacrificial anionic surfactant with high HOMO energy level as a general descriptor for zinc anode. *Energy Storage Mater.* **2024**, *70*, 103525.
(7) Lv, W.; Meng, J.; Li, Y.; Yang, W.; Tian, Y.; Lyu, X.; Duan, C.; Ma, X.; Wu, Y. Inexpensive and eco-friendly nanostructured birnessite-type δ-MnO2: A design strategy from oxygen defect engineering and K+ pre-intercalation. *Nano Energy* **2022**, *98*, 107274.
(8) Du, H.; Yi, Z.; Li, H.; Lv, W.; Hu, N.; Zhang, X.; Chen, W.; Wei, Z.; Shen, F.; He, H. Separator Design Strategies to Advance Rechargeable Aqueous Zinc Ion Batteries. *Chem.—Eur. J.* **2024**, *30*, 202303461.
(9) Zheng, X.; Ahmad, T.; Chen, W. Challenges and strategies on Zn electrodeposition for stable Zn-ion batteries. *Energy Storage Mater.* **2021**, *39*, 365−394.
(10) Guo, Y.; Zhang, Y.; Lu, H. Manganese-based materials as cathode for rechargeable aqueous zinc-ion batteries. *Battery Energy* **2022**, *1*, 20210014.
(11) Meng, Y.; Wang, M.; Wang, J.; Huang, X.; Zhou, X.; Sajid, M.; Xie, Z.; Luo, R.; Zhu, Z.; Zhang, Z.; Khan, N.; Wang, Y.; Li, Z.; Chen, W. Robust bilayer solid electrolyte interphase for Zn electrode with high utilization and efficiency. *Nat. Commun.* **2024**, *15*, 8431.
(12) Li, D.; Zhong, Y.; Xu, X.; Zhou, D.; Tang, Y.; Wang, L.; Liang, S.; Lu, B.; Liu, Y.; Zhou, J. Reinforcing the symmetry of stripping/plating behavior via in situ interface construction for long-lasting zinc metal batteries. *Energy Environ. Sci.* **2024**, *17*, 8855−8865.
(13) Lv, W.; Meng, J.; Li, X.; Xu, C.; Yang, W.; Duan, S.; Li, Y.; Ju, X.; Yuan, R.; Tian, Y.; Wang, M.; Lyu, X.; Pan, P.; Ma, X.; Cong, Y.; Wu, Y. Boosting zinc storage in potassium-birnessite via organic-inorganic electrolyte strategy with slight N-methyl-2-pyrrolidone additive. *Energy Storage Mater.* **2023**, *54*, 784.
(14) Lv, W.; Shen, Z.; Li, X.; Meng, J.; Yang, W.; Ding, F.; Ju, X.; Ye, F.; Li, Y.; Lyu, X.; Wang, M.; Tian, Y.; Xu, C. Discovering Cathodic Biocompatibility for Aqueous Zn-MnO2 Battery: An Integrating Biomass Carbon Strategy. *Nano-Micro Lett.* **2024**, *16*, 109.
(15) Xie, C.; Li, Y.; Wang, Q.; Sun, D.; Tang, Y.; Wang, H. Issues and solutions toward zinc anode in aqueous zinc-ion batteries: A mini review. *Carbon Energy* **2020**, *2*, 540−560.
(16) Zhang, W.; Zhu, X.; Kang, L.; Peng, Z.; Zhu, J.; Pan, L.; Dai, L.; Liu, S.; Wang, L.; Liu, Y.; He, Z. Stabilizing zinc anode using zeolite imidazole framework functionalized separator for durable aqueous zinc-ion batteries. *J. Energy Chem.* **2024**, *90*, 23−31.
(17) Ding, F.; Xu, W.; Graff, G. L.; Zhang, J.; Sushko, M. L.; Chen, X.; Shao, Y.; Engelhard, M. H.; Nie, Z.; Xiao, J.; Liu, X.; Sushko, P. V.; Liu, J.; Zhang, J. G. Dendrite-free lithium deposition via self-healing electrostatic shield mechanism. *J. Am. Chem. Soc.* **2013**, *135*, 4450.
(18) Zheng, J.; Huang, Z.; Zeng, Y.; Liu, W.; Wei, B.; Qi, Z.; Wang, Z.; Xia, C.; Liang, H. Electrostatic Shielding Regulation of Magnetron Sputtered Al-Based Alloy Protective Coatings Enables Highly Reversible Zinc Anodes. *Nano Lett.* **2022**, *22*, 1017.

(19) Zhou, J.; Li, Q.; Hu, X.; Wei, W.; Ji, X.; Kuang, G.; Zhou, L.; Chen, L.; Chen, Y. Water molecules regulation for reversible Zn anode in aqueous zinc ion battery: Mini-review. *Chin. Chem. Lett.* **2024**, *35*, 109143.
(20) Wu, S.; Hu, Z.; He, P.; Ren, L.; Huang, J.; Luo, J. Crystallographic engineering of Zn anodes for aqueous batteries. *eScience* **2023**, *3*, 100120.
(21) Zhou, J.; Li, Q.; Hu, X.; Wei, W.; Ji, X.; Kuang, G.; Zhou, L.; Chen, L.; Chen, Y. Water molecules regulation for reversible Zn anode in aqueous zinc ion battery: Mini-review. *Chin. Chem. Lett.* **2024**, *35*, 109143.
(22) Wang, F.; Borodin, O.; Gao, T.; Fan, X.; Sun, W.; Han, F.; Faraone, A.; Dura, J. A.; Xu, K.; Wang, C. Highly reversible zinc metal anode for aqueous batteries. *Nat. Mater.* **2018**, *17*, 543−549.
(23) Cheng, Z.; Wang, K.; Fu, J.; Mo, F.; Lu, P.; Gao, J.; Ho, D.; Li, B.; Hu, H. Texture Exposure of Unconventional (101)Zn Facet: Enabling Dendrite-Free Zn Deposition on Metallic Zinc Anodes. *Adv. Energy Mater.* **2024**, *14*, 2304003.
(24) Chen, R.; Zhang, W.; Huang, Q.; Guan, C.; Zong, W.; Dai, Y.; Du, Z.; Zhang, Z.; Li, J.; Guo, F.; Gao, X.; Dong, H.; Zhu, J.; Wang, X.; He, G. Trace Amounts of Triple-Functional Additives Enable Reversible Aqueous Zinc-Ion Batteries from a Comprehensive Perspective. *Nano-Micro Lett.* **2023**, *15*, 81.
(25) Zhao, R.; Yang, Y.; Liu, G.; Zhu, R.; Huang, J.; Chen, Z.; Gao, Z.; Chen, X.; Qie, L. Redirected Zn Electrodeposition by an Anti-Corrosion Elastic Constraint for Highly Reversible Zn Anodes. *Adv. Funct. Mater.* **2021**, *31*, 2001867.
(26) Hao, J.; Li, X.; Zhang, S.; Yang, F.; Zeng, X.; Zhang, S.; Bo, G.; Wang, C.; Guo, Z. Designing Dendrite-Free Zinc Anodes for Advanced Aqueous Zinc Batteries. *Adv. Funct. Mater.* **2020**, *30*, 2001263.
(27) Hao, J.; Li, B.; Li, X.; Zeng, X.; Zhang, S.; Yang, F.; Liu, S.; Li, D.; Wu, C.; Guo, Z. An In-Depth Study of Zn Metal Surface Chemistry for Advanced Aqueous Zn-Ion Batteries. *Adv. Mater.* **2020**, *32*, 2003021.
(28) Kang, L.; Cui, M.; Jiang, F.; Gao, Y.; Luo, H.; Liu, J.; Liang, W.; Zhi, C. Nanoporous CaCO3 Coatings Enabled Uniform Zn Stripping/Plating for Long-Life Zinc Rechargeable Aqueous Batteries. *Adv. Energy Mater.* **2018**, *8*, 1801090.
(29) Deng, C.; Xie, X.; Han, J.; Tang, Y.; Gao, J.; Liu, C.; Shi, X.; Zhou, J.; Liang, S. A Sieve-Functional and Uniform-Porous Kaolin Layer toward Stable Zinc Metal Anode. *Adv. Funct. Mater.* **2020**, *30*, 2000599.
(30) Parker, J. F.; Chervin, C. N.; Pala, I. R.; Machler, M.; Burz, M. F.; Long, J. W.; Rolison, D. R. Rechargeable nickel-3D zinc batteries: An energy-dense, safer alternative to lithium-ion. *Science* **2017**, *356*, 415−418.
(31) Guo, N.; Huo, W.; Dong, X.; Sun, Z.; Lu, Y.; Wu, X.; Dai, L.; Wang, L.; Lin, H.; Liu, H.; Liang, H.; He, Z.; Zhang, Q. A Review on 3D Zinc Anodes for Zinc Ion Batteries. *Small Methods* **2022**, *6*, No. e2200597.
(32) Xu, K.; Zheng, X.; Luo, R.; Sun, J.; Ma, Y.; Chen, N.; Wang, M.; Song, L.; Zhao, Q.; Chen, W. A three-dimensional zincophilic nano-copper host enables dendrite-free and anode-free Zn batteries. *Mater. Today Energy* **2023**, *34*, 101284.
(33) Gong, Y.; Wang, B.; Ren, H.; Li, D.; Wang, D.; Liu, H.; Dou, S. Recent Advances in Structural Optimization and Surface Modification on Current Collectors for High-Performance Zinc Anode: Principles, Strategies, and Challenges. *Nano-Micro Lett.* **2023**, *15*, 208.
(34) Zheng, X.; Liu, Z.; Sun, J.; Luo, R.; Xu, K.; Si, M.; Kang, J.; Yuan, Y.; Liu, S.; Ahmad, T.; Jiang, T.; Chen, N.; Wang, M.; Xu, Y.; Chuai, M.; Zhu, Z.; Peng, Q.; Meng, Y.; Zhang, K.; Wang, W.; Chen, W. Constructing robust heterostructured interface for anode-free zinc batteries with ultrahigh capacities. *Nat. Commun.* **2023**, *14*, 76.
(35) Li, R.; Du, Y.; Li, Y.; He, Z.; Dai, L.; Wang, L.; Wu, X.; Zhang, j.; Yi, J. Alloying Strategy for High-Performance Zinc Metal Anodes. *ACS Energy Lett.* **2023**, *8*, 457−476.
(36) Zhang, Y.; Howe, J. D.; Ben-Yoseph, S.; Wu, Y.; Liu, N. Unveiling the Origin of Alloy-Seeded and Nondendritic Growth of Zn for Rechargeable Aqueous Zn Batteries. *ACS Energy Lett.* **2021**, *6*, 404−412.
(37) Zhang, Y.; Wang, G.; Yu, F.; Xu, G.; Li, Z.; Zhu, M.; Yue, Z.; Wu, M.; Liu, H.-K.; Dou, S.-X.; Wu, C. Highly reversible and dendrite-free Zn electrodeposition enabled by a thin metallic interfacial layer in aqueous batteries. *Chem. Eng. J.* **2021**, *416*, 128062.
(38) Yi, Z.; Liu, J.; Tan, S.; Sang, Z.; Mao, J.; Yin, L.; Liu, X.; Wang, L.; Hou, F.; Dou, S. X.; Cheng, H. M.; Liang, J. An Ultrahigh Rate and Stable Zinc Anode by Facet-Matching-Induced Dendrite Regulation. *Adv. Mater.* **2022**, *34*, 2203835.
(39) Zhou, M.; Guo, S.; Li, J.; Luo, X.; Liu, Z.; Zhang, T.; Cao, X.; Long, M.; Lu, B.; Pan, A.; Fang, G.; Zhou, J.; Liang, S. Surface-Preferred Crystal Plane for a Stable and Reversible Zinc Anode. *Adv. Mater.* **2021**, *33*, No. e2100187.
(40) Zhao, C.; Sun, J.; Lu, W.; Sun, P.; Wu, M.; Lian, R.; Wang, Y.; Wei, Y. Microscopic Insights into Zn (002) Epitaxial Electrodeposition in Aqueous Zinc Metal Batteries. *Nano Lett.* **2024**, *24*, 16408.
(41) Xiao, X.; Greenburg, L. C.; Li, Y.; Yang, M.; Tzeng, Y.-K.; Sui, C.; Peng, Y.; Wu, Y.; Zhang, Z.; Gao, X.; Xu, R.; Ye, Y.; Zhang, P.; Yang, Y.; Vailionis, A.; Hsu, P.-c.; Qin, J.; Cui, Y. Epitaxial Electrodeposition of Zinc on Different Single Crystal Copper Substrates for High Performance Aqueous Batteries. *Nano Lett.* **2025**, *25*, 1305.
(42) Wang, J.; Cai, Z.; Xiao, R.; Ou, Y.; Zhan, R.; Yuan, Z.; Sun, Y. A Chemically Polished Zinc Metal Electrode with a Ridge-like Structure for Cycle-Stable Aqueous Batteries. *ACS Appl. Mater. Interfaces* **2020**, *12*, 23028.
(43) Wang, S.-B.; Ran, Q.; Yao, R.-Q.; Shi, H.; Wen, Z.; Zhao, M.; Lang, X.-Y.; Jiang, Q. Lamella-nanostructured eutectic zinc-aluminum alloys as reversible and dendrite-free anodes for aqueous rechargeable batteries. *Nat. Commun.* **2020**, *11*, 1634.
(44) Wu, Z.; Zou, J.; Li, Y.; Hansen, E. J.; Sun, D.; Wang, H.; Wang, L.; Liu, J. Regulating Zinc Nucleation Sites and Electric Field Distribution to Achieve High-Performance Zinc Metal Anode via Surface Texturing. *Small* **2023**, *19*, 2206634.
(45) Liu, H.; Zhang, Y.; Wang, C.; Glazer, J. N.; Shan, Z.; Liu, N. Understanding and Controlling the Nucleation and Growth of Zn Electrodeposits for Aqueous Zinc-Ion Batteries. *ACS Appl. Mater. Interfaces* **2021**, *13*, 32930.
(46) Hou, Z.; Gao, Y.; Zhou, R.; Zhang, B. Unraveling the Rate-Dependent Stability of Metal Anodes and Its Implication in Designing Cycling Protocol. *Adv. Funct. Mater.* **2022**, *32*, 2107584.
(47) Qian, G.; Zan, G.; Li, J.; Lee, S. J.; Wang, Y.; Zhu, Y.; Gul, S.; Vine, D. J.; Lewis, S.; Yun, W.; Ma, Z. F.; Pianetta, P.; Lee, J. S.; Li, L.; Liu, Y. Structural, Dynamic, and Chemical Complexities in Zinc Anode of an Operating Aqueous Zn-Ion Battery. *Adv. Energy Mater.* **2022**, *12*, 2200255.
(48) Zhu, Z.; Lu, L.-L.; Yin, Y.; Shao, J.; Shen, B.; Yao, H.-B High Rate and Stable Solid-State Lithium Metal Batteries Enabled by Electronic and Ionic Mixed Conducting Network Interlayers. *ACS Appl. Mater. Interfaces* **2019**, *11*, 16578−16585.
(49) Lu, L. L.; Zhu, Z. X.; Ma, T.; Tian, T.; Ju, H. X.; Wang, X. X.; Peng, J. L.; Yao, H. B.; Yu, S. H. Superior Fast-Charging Lithium-Ion Batteries Enabled by the High-Speed Solid-State Lithium Transport of an Intermetallic Cu_6Sn_5 Network. *Adv. Mater.* **2022**, *34*, No. e2202688.
(50) Wang, C.; Ping, W.; Bai, Q.; Cui, H.; Hensleigh, R.; Wang, R.; Brozena, A. H.; Xu, Z.; Dai, J.; Pei, Y.; Zheng, C.; Pastel, G.; Gao, J.; Wang, X.; Wang, H.; Zhao, J.-C.; Yang, B.; Zheng, X.; Luo, J.; Mo, Y.; Dunn, B.; Hu, L. A general method to synthesize and sinter bulk ceramics in seconds. *Science* **2020**, *368*, 521−526.
(51) Dong, Q.; Yao, Y.; Cheng, S.; Alexopoulos, K.; Gao, J.; Srinivas, S.; Wang, Y.; Pei, Y.; Zheng, C.; Brozena, A. H.; Zhao, H.; Wang, X.; Toraman, H. E.; Yang, B.; Kevrekidis, I. G.; Ju, Y.; Vlachos, D. G.; Liu, D.; Hu, L. Programmable heating and quenching for efficient thermochemical synthesis. *Nature* **2022**, *605*, 470−476.
(52) Song, J.; Kim, M.-R.; Kim, Y.; Seo, D.; Ha, K.; Song, T.-E.; Lee, W.-G.; Lee, Y.; Kim, K.-C.; Ahn, C. W.; Han, H. Fabrication of junction-free Cu nanowire networks via Ru-catalyzed electroless deposition and their application to transparent conducting electrodes. *Nanotechnology* **2022**, *33*, 065303.
(53) Li, Y.; Wu, P.; Zhong, W.; Xie, C.; Xie, Y.; Zhang, Q.; Sun, D.; Tang, Y.; Wang, H. A progressive nucleation mechanism enables stable

https://doi.org/10.1021/acs.nanolett.4c06347
Nano Lett. XXXX, XXX, XXX−XXX

zinc stripping-plating behavior. *Energy Environ. Sci.* **2021**, *14*, 5563−5571.

https://doi.org/10.1021/acs.nanolett.4c06347
Nano Lett. XXXX, XXX, XXX−XXX